# Development and Evaluation of Autonomous Mobile Manipulator for Large Scale Outdoor Environment

Takeshi OHKI, Kiichi SATO, Keiji NAGATANI and Kazuya YOSHIDA

*Abstract*— **Recently, there has been rapid progress in the development of nondestructive sensing method for underground structures using artificial earthquake and seismometer array technology. However, this requires the deployment of many sensing devices over a wide area on a target outdoor field; such work is currently conducted in manually. To automate such work, our research group has been developing an autonomous mobile manipulator system for automatic rather than manual deployment of sensing devices. To realize such a deployment, the important technical issues are "mobility on rough terrain," "3D localization," and "manipulation." In this research, we designed and implemented these functions in our mobile manipulator system, called "El-Verde," and conducted field tests to validate its capability and to identify problems when applied in a real environment. In this paper, we introduce its implementation and report the field-test results.**

## I. INTRODUCTION

### A. Background

Even though there is a strong movement to break away from a fossil-fuel society, there will still be a large demand for oil exploration activities throughout the world. Therefore, a nondestructive method of sensing underground structures to find oilfields is required. One of the methods, which involves the use of artificial earthquake and seismometer array technology to detect such structures, has become very popular. However, detecting the reflections of earthquake waves in different locations requires the deployment of many sensing devices over the wide area in the target field, which is currently done manually. To reduce the workloads on humans, there is a strong demand to realize a robotic sensor deployment system for outdoor environments. Thus, our research group initiated a project to realize such a system and developed an autonomous mobile manipulator; we conducted experiments to validate our system.

With regard to mobile manipulation, there has been several past studies on autonomous mobile manipulators [1][2][3]. However, almost all were for indoor use. Focusing on mobility in outdoor fields, our research group has reported many field tests, such as those in simulated disaster areas[4][5], underground malls[6], and volcanic sites. Based on our experiences, we believe that we can realize an autonomous mobile manipulator that performs well in outdoor environments.

Manuscript received October 11, 2011.

T. Ohki, K. Sato, K. Nagatani and K. Yoshida are with the Department of Aerospace Engineering, Graduate School of Engineering, Tohoku University, Aramaki aza Aoba 6-6-01, Sendai 980-8579, JAPAN {takeshi,kiichi,keiji,yoshida}@astro.mech.tohoku.ac.jp

### B. Research Purpose

The aim of this research is to develop a robotic system for autonomous deployment of sensing devices in an outdoor field. To perform such a deployment task, we pre-defined a specific scenario for the mobile manipulator system as follows.

1) The mobile base moves to the closest location, that is called the "target point," to set a sensing device.
2) It stops and places the end-effector at a location above the target point by precise control of the mounted manipulator.
3) It installs the sensing device at the target point.
4) It brings the manipulator back to the initial configuration.
5) Repeat 1-4 are repeated until all sensing devices have been installed.

In the scenario, we assume that (a) the target environment is wide, roughly flat outdoor area, (b) the robot has information on the target environment, (c) the locations of the target points are given in advance, and (d) the robot is equipped with a manipulator and sensing devices. To achieve the above scenario, we considered the important technical issues to be "mobility on rough terrain," "localization," and "manipulation." We designed and implemented a prototype of an autonomous mobile manipulator system called "El-Verde," and conducted field tests to validate its capability and to identify problems in field application.

## II. STRATEGY AND KEY FEATURES

To realize the scenario presented in the previous section, three key issues of "mobility," "localization," and "manipulation" are quite important.

Mobility, is the foundation of mobile manipulators. The manipulator should not only be capable of traversing rough terrain but mechanisms for achieving the same should also be simple. In this study, we chose to equip the robot with a rocker link suspension to traverse rough terrains, as described in the next section.

Localization means to obtain the current position of the mobile base. To direct the end-effector to the desired position, localization is the most important issue. For stable localization method of the base robot, we implemented gyroscope-based odometry and particle filtering technology in this study.

Manipulation involves navigating the end-effector of the mounted manipulator to the target points. Usually, the workspace region of the manipulator is limited when the

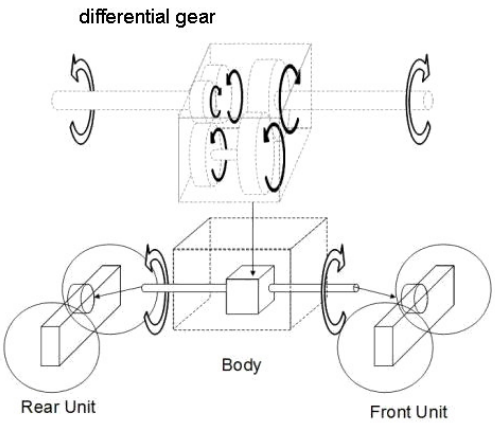


Fig. 1. Rocker link suspension

Fig. 2. Autonomous mobile manipulator "El-Verde"

base robot is stationary. Therefore, the base robot should be navigated to near the target points beforehand, after which, the end-effector is navigated to a target point precisely, as described in section V.

## III. MOBILITY SYSTEM

A number of suspension systems for mobile robots to traverse rough terrains have been proposed. The rocker-bogie suspension mechanism (Fig. 1) is a well-known suspension system used for NASA's Mars rover, that was developed at Jet Propulsion Laboratory (JPL) [7]. By rocking the link passively, this simple mechanism enhances the mobility of the robot, enabling it to surmount obstacles with heights similar to the diameter of its wheels. The rocker link suspension connects the center body with the rear unit and front unit by a single axis. A differential gear is employed, because of which when the front unit rotates around the axis, the rear unit rotates around the axis at the same angle in the reverse direction. The rocker link allows the four wheels to maintain contact on rough terrains.

Fig. 2 shows the developed mobile robot called "El-Verde." The mobile robot has four wheels with the independent actuators and the Ackerman steering mechanism mounted on the front part of the robot. Therefore, the robot is moved by the five actuators.

## IV. LOCALIZATION

### A. Gyro-Based Odometry

Localization refers to technology for accurately determining the current position of a mobile robot. The most basic method of localization is called "wheel odometry"; in this method, a wheel encoder counts the rotations of the wheels of mobile robots. Wheel odometry is used to estimate the current position by periodically accumulating the translational velocity and turning angular velocity based on the left and right wheel rotation velocities. However, wheel odometry only calculates the location of the robot in two-dimensional space; the outdoor environments we are targeting are three-dimensional (3-D) rough terrains.

Therefore, in our approach, we use "gyro-based odometry" [8], that combines the wheel odometry with 3-D angle information from onboard three gyroscopes. Gyro-based odometry is calculated by the following equations where $\triangle t$ is the sampling time, $v_n$ is the transitional velocity obtained by wheels encoders, $\theta_n$ is the accumulated yaw angle, and $\phi_n$ is the accumulated pitch angle as calculated by the gyroscopes.

$$x_n = v_n cos(\theta_n) cos(\phi_n) \triangle t + x_{n-1} \quad (1)$$

$$y_n = v_n sin(\theta_n) cos(\phi_n) \triangle t + y_{n-1} \quad (2)$$

$$z_n = v_n sin(\phi_n) \triangle t + z_{n-1} \quad (3)$$

The transitional velocity $v_n$ is derived from the average velocity of the rear wheel pair because when the robot turns, the velocity fluctuations are more rapid for the front wheel pair than for the rear wheel pair.

The 3-D posture of the robot is derived by using three gyroscopes. However, temperature changes can causes errors in the information provided by a gyroscope. The errors accumulated as the 3-D posture are calculated, and they are called the temperature drift error. To cancel the temperature drift errors, we incorporate the drift canceling algorithm by using a three degrees of freedom (3-D.O.F) acceleration sensor [8] that identifies whether the robot has stopped or not and cancels the drift when it has. However, error accumulation by the gyro wheel odometry with regard to the robot's position due to slipping of the wheels is unavoidable, especially on rough terrain.

### B. Particle Filter

To cancel the accumulated localization errors, we use the particle filter algorithm [9]. The particle filter is a time series filter based on the Monte Carlo method (MC); it is a famous position estimation method for mobile robots and widely used. By using the particle filter, we combine the 3-D gyro-based odometry and "GPS position," that is the position calculated by using GPS information, to get more accurate 3-D odometry.

Although there are still limits to the positioning accuracy of GPS, it is globally correct, and there are no accumulated

errors, unlike in gyro-based odometry, except when there are obstacles between the GPS antenna and GPS satellites or when GPS signal reflections occur next to flat obstacles, such as tall buildings. Conversely, gyro-based odometry is locally more accurate than GPS although it has the drawback of error accumulation. By combining gyro-based odometry and GPS positioning, the advantages of the both positioning methods are combined.

The algorithm of the particle filter we implemented repeats the following procedure periodically at a constant frequency.

1) Initialization phase: Prepare initial 1024 particles for the hypothetical odometry.
2) Prediction phase: Predict all of the particles from the changes in the gyro-based odometry with random errors.
3) GPS check phase: If the GPS position is not updated or there is an unusual jump, go back to the prediction phase. Otherwise, go to the next phase.
4) Weighting phase: Derive the likelihood $\omega_t^{[i]}$ for $particles[i]_t$ based on the errors between the particle and GPS position by using Equation (4).
5) Resampling phase: Resample the particles based on the normalized likelihood $\omega_t^{[i]}$ for each $particle[i]_t$ by selecting randomly within the accumulated weights of all the particles.
6) Averaging phase: Calculate an average particle for the filtered odometry.

$$\omega_t^{[i]} = \frac{1}{\sqrt{2\pi}\sigma_{GPS}} \exp\left(\frac{-d^{[i]2}}{2\sigma_{GPS}^2}\right) \quad (4)$$

where $d_t^{[i]}$ is the error between $particle[i]$ and the GPS position, $\sigma_{GPS}$ is the standard deviation of GPS positions.

By using the above algorithm, the 2-D coordinates $x, y$ and yaw angle $\theta_{yaw}$ of the mobile robot are modified by the particle filter, Other parameters such as the vertical position $z$, pitch angle $\theta_{pitch}$, and rolling angle $\theta_{roll}$, are calculated by the gyro-based odometry. We call this odometry as "particle-filtered gyro-based odometry."

### C. Implementation

We implemented the gyro-based odometry within the motor controller with three gyro sensors and an acceleration sensor. The odometry is calculated every 25 msec. In addition, the particle filter was implemented on the main onboard PC, and the particle-filtered gyro-based odometry is updated every 100 msec. By considering the GPS position accuracy, $\sigma_{GPS}$ is empirically derived as 1 m. The GPS position is obtained almost every second.

The GPS coordinates correspond to the world coordinates. The X-axis refers to the east direction, the Y-axis refers to the north direction, and the origin is the initial position of the robot. The coordinates of the gyro-based odometry are the local coordinates where the X-axis is the initial direction of the robot, and the Y-axis is orthogonal to the X-axis.

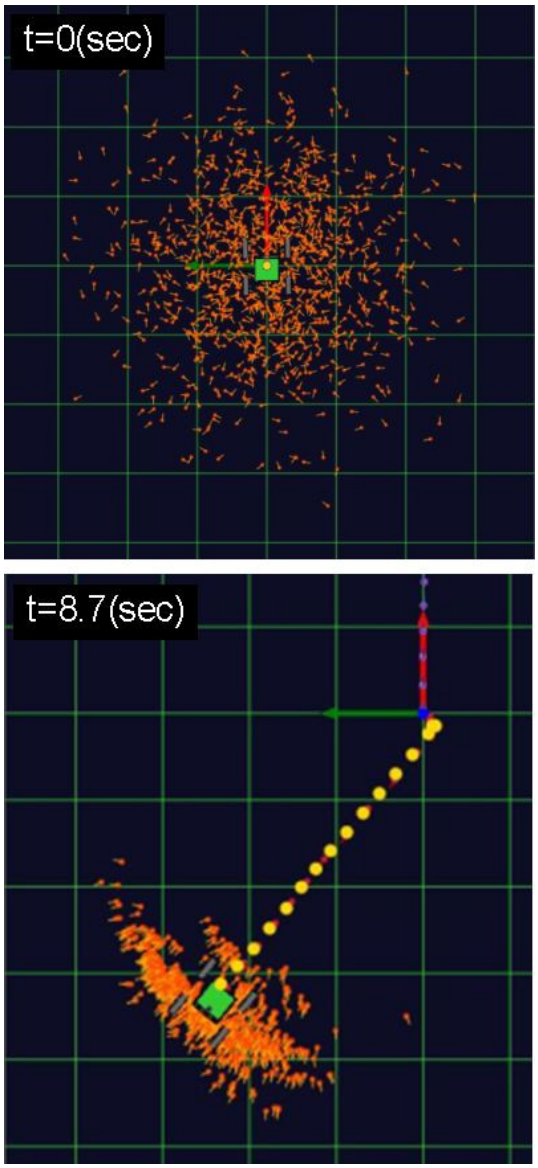


Fig. 3. Convergence of particles

An example of the visualized particle is shown in Fig. 3, where the red and green arrows donate X and Y axes respectiovely, of the local and the world coordinates; the orange dots express each particle; the yellow dots express the GPS positions; and the blue dots are the gyro-based odometry. This figure shows the convergence of the particles by GPS positions with time.

## V. MANIPULATION

### A. Hardware

Fig. 4 shows the mounted manipulator for our mobile robot, that is a 3 D.O.F scalar-type manipulator. The first and second joints of this manipulator control the horizontal motion of the end-effector, and the third joint is for vertical motion when deploying the sensing devices. Link1 is 395 mm long, and link2 is 610 mm long. The maximum reach

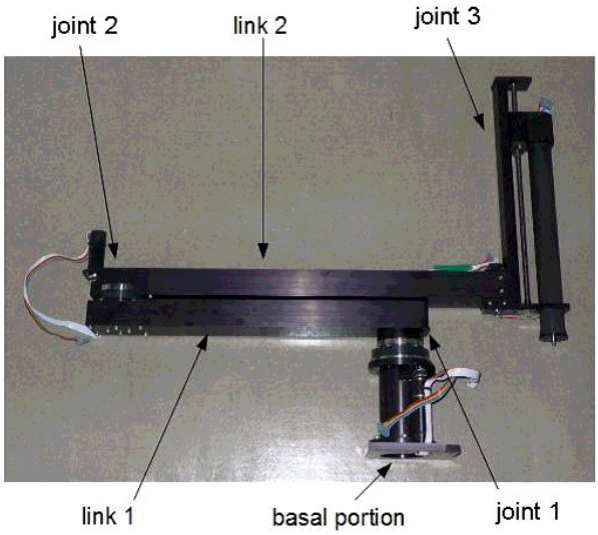


Fig. 4. 3-D.O.F. manipulator

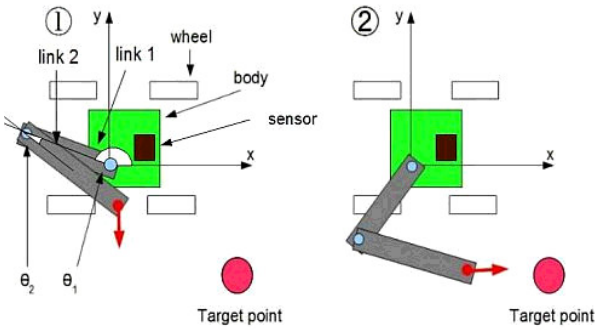


Fig. 5. Motion of manipulator

of the end-effector is almost 1 m on a planar surface from the coordinates of the origin. The manipulator is attached to the center body of the mobile robot, as shown in Fig. 2.

### B. Control Scheme

The control scheme for the manipulation has two parts; navigation of the base robot, that the base robot is navigated to the left side of near the closest target point, and navigation of the mounted manipulator, that the end-effector is precisely navigated to the target point.

Fig. 5 shows the navigation sequence for the mounted manipulator. In this figure, the red dot expresses the position of the end-effector, that is called "end position." The target point is located on the right side of the robot because the base robot is navigated to the left side of the target.

The initial angle state of the manipulator is shown in Fig. 5. $\theta_1$ is the angle from the X-axis to the direction of link 1 anticlockwise, and $\theta_2$ is the angle from the direction of link 1 to the direction of link 2 anticlockwise also. The state where $\theta_1$ and $\theta_2$ are 180 deg and 0 deg respectively, is the singular solution of the 2-D.O.F. planar manipulator. To avoid the singular posture, the initial angles of $\theta_1$ and $\theta_2$ are set as 150 deg and -15 deg respectively.

To prevent link 1 of the manipulator from colliding with the onboard sensor on top of the center body of the robot, $\theta_1$ is limited to values of between 0 deg and 90 deg. Also, to prevent the end-effector from colliding with the wheels, the initial motion at the initial angular state transits through a state called "middle state" (the left side of Fig. 5), and then, the end position is then navigated to the target point (right side of Fig. 5).

Next, by sliding the end position vertically, the sensing devices are deployed. After deployment, the end-effector is navigated to the initial position via the middle state.

The motions of the manipulator in the states shown in Fig. 5 are controlled by the angular velocities of the each joint as expressed by $\dot{q}(\dot{\theta}_1, \dot{\theta}_2)$. $\dot{q}(\dot{\theta}_1, \dot{\theta}_2)$ is derived by the following equation.

$$\dot{q} = J^{-1}\dot{r} \tag{5}$$

where

$$J = \begin{pmatrix} -l_1 cos(\theta_1) - l_2 sin(\theta_1 + \theta_2) & -l_2 sin(\theta_1 + \theta_2) \\ l_2 cos(\theta_1) + l_2 cos(\theta_1 + \theta_2) & l_2 cos(\theta_1 + \theta_2) \end{pmatrix}$$

$l_1$ is the length of link 1 and $l_2$ is the length of link 2. $\dot{r}(\dot{x}, \dot{y})$ is the velocity vector from the current "end position" to the destination.

## VI. EXPERIMENTS

### A. Experimental Procedure

To confirm the validity of our integration, we conducted two types of experiments according to the above-described scenario. In these experiments, the input information is the list of target points defined by the operators, and each process of the scenario transits automatically when the remote operator gives permission.

To evaluate the position errors between the set targets and deployed positions in the experiments, a laser measurement tool called a "total station" that can measure the 3-D position of a prism reflector was used. The total station measures the 3-D position by combining the distance to the prism and the direction in which the prism is located. The distance is measured by optical wave ranging, and the direction is measured by a theodolite. The accuracy of the 3-D position, as measured by the total station, is $\pm 1$ cm.

To detect the end position, the reflector of the total station is attached to the top of the slider of the manipulator. By using the total station, the trajectories of the end position can be obtained every 0.3 sec.

### B. Target Environment

The target environment for these experiments was along the Hirose River in Sendai, that is shown in Fig. 6. In this paper, we report the results of two types of experiments. One used straight targets, as shown in Fig. 6-(a), and is called the "straight experiment"; the other used zigzag targets, as shown in Fig. 6-(b), and is called the "zigzag experiment." In the straight experiment, the distance between the target points

(a) straight experiment

(b) zigzag experiment

Fig. 6. Target points on an outdoor field

is 10 m. In the zigzag experiment, the distance between the target points is 10 m for the initial direction of the robot and 5 m along the direction orthogonal to the initial direction of the robot. The environment is almost flat and there are no large obstacles that the robot has to avoid by changing its path.

### C. Result

The blue dots in Fig. 7 and Fig. 8 are the trajectories measured by the total station, and the pink dots are the measured deployed points. Because of limitations with the wireless network, the straight experiment was finished at a distance of 170 m from the initial position, and the zigzag experiment was finished at a distance of around 70 m from the initial position. In Fig. 7 and Fig. 8, the initial positions of the coordinates are set as the initial position of the robot. In addition, the direction of the X-axis in the figures are adjusted as the initial direction of the robot by using the two deployed positions. During the sixth deployment in the zigzag experiment, the reflector could not be detected by the total station because the reflector was hidden on the far side of the robot itself.

Fig. 9 and Fig. 10 show the errors between the set target points and the deployed positions, and the origins of the coordinates donates the center positions of the errors. In the straight experiment, the standard deviation of the X-axis is 58 mm, and that of the Y-axis is 148 mm. In the zigzag experiment, the standard deviation of the X-axis is 283 mm, and that of the Y-axis is 123 mm.

### D. Discussion

The manipulation methods in the two experiments are same, therefore, we assume that the manipulation accuracy in the two experiments would be almost the same. However, the errors in the zigzag experiments has larger standard deviations than those in the straight experiment. This is because the robot has to turn more frequently in the zigzag experiment than in the straight experiment, that may have caused errors in the odometry. Therefore, the results of the two experiments are reasonable.

Of the samples, 99.7 % are within the three times the value of the defined standard deviation, from its definition. The maximum standard deviation from both experiments is 283 mm in the zigzag experiment. Therefore, we assume that 99.7 % of the deployments are performed within 849 mm by using our system.

The positioning accuracy of the GPS we used is larger than 1 m. Even when the GPS is set in differential GPS mode, the accuracy is still almost 1 m. The experimental results confirmed the validity of our system.

## VII. CONCLUSION AND FUTURE WORKS

### A. Conclusion

To realize autonomous sensing device deployment, we designed an autonomous mobile manipulator system. This paper presents the integration of the high-mobility system, the particle-filtered gyro-based odometry and the manipulation. In the two types of experiments, our system performed 99.7 % of the deployments within 849 mm of the target points. The experimental results confirmed the validity of our system.

### B. Future Works

Currently, the robot stops during the deployment procedure. To reduce the deployment time, the manipulation and traversing path planning should be performed simultaneously. In addition, the development of a collision avoidance algorithm to avoid large obstacles during the traversing is also desirable.

## REFERENCES

[1] K. Nagatani and S. Yuta, "An experiment on opening-door-behavior by an autonomous mobile robot with a manipulator," in *IEEE/RSJ International Conference on Intelligent Robots and Systems*, vol. 2, pp. 45 –50, Aug 1995.

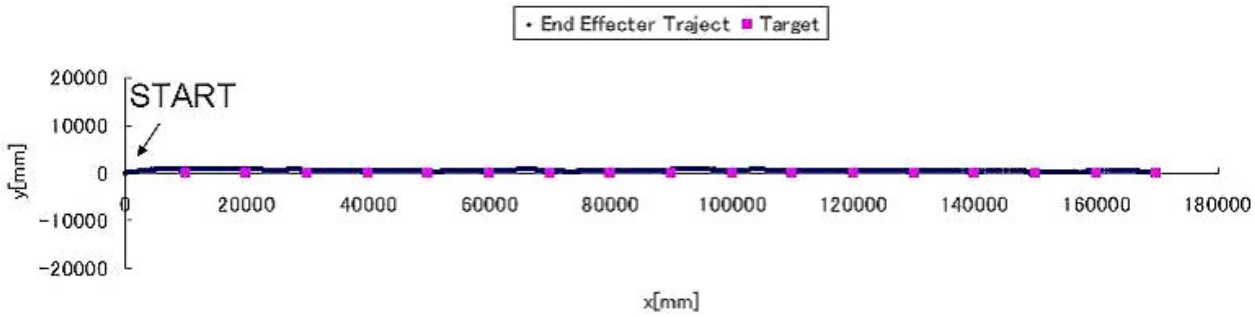


Fig. 7. Trajectory of end-effector in straight experiment

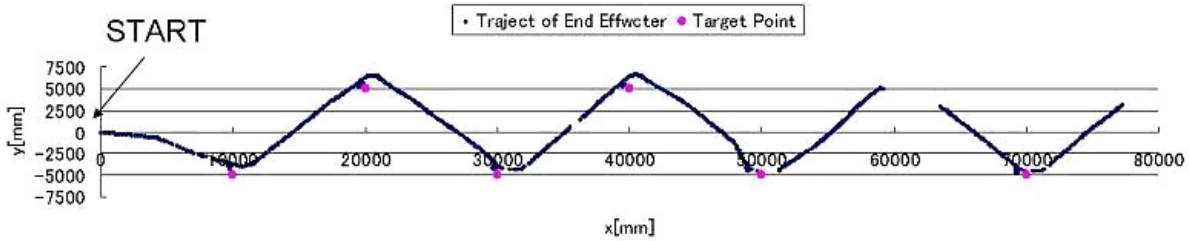


Fig. 8. Trajectory of end-effector in zigzag experiment

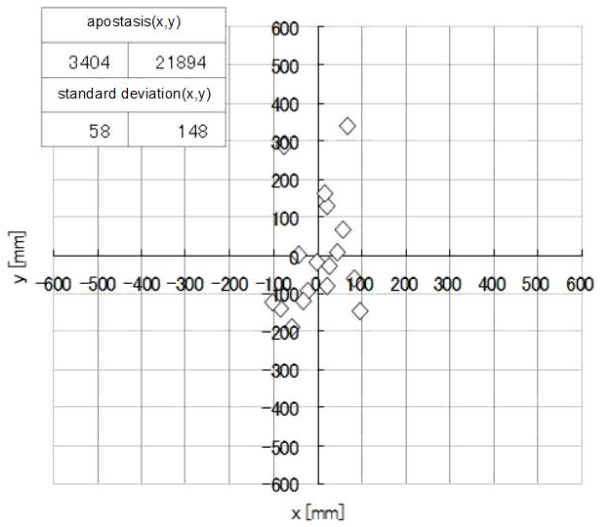


Fig. 9. Errors of deployed positions in straight experiment

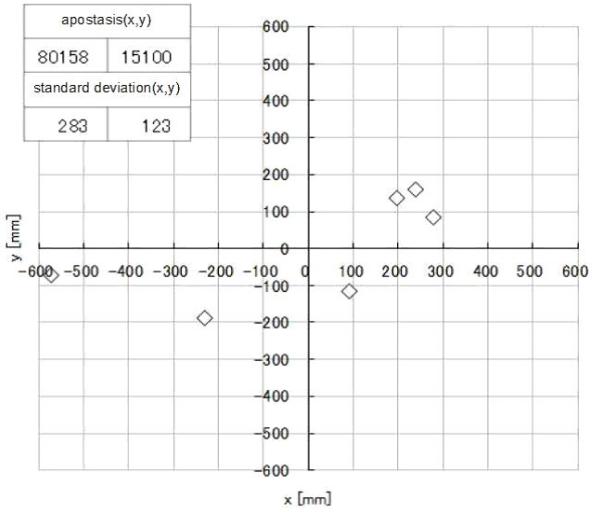


Fig. 10. Errors of deployed positions in zigzag experiment


[2] E. Van Henten, "Field test of an autonomous cucumber picking robot," *Biosystems Engineering*, vol. 86, no. 3, pp. 305–313, 2003.

[3] D. Katz, E. Horrell, O. Yang, B. Burns, T. Buckley, A. Grishkan, V. Zhylkovskyy, O. Brock, and E. Learned-Miller, "The umass mobile manipulator uman: An experimental platform for autonomous mobile manipulation," in *Workshop on Manipulation in Human Environments at Robotics: Science and Systems*, 2006.

[4] T. Ohki, K. Nagatani, and K. Yoshida, "Collision avoidance method for mobile robot considering motion and personal spaces of evacuees," in *Proc. of IEEE/RSJ International Conference on Intellegent Robots and Systems*, 2010.

[5] T. Ohki, K. Nagatani, and K. Yoshida, "Safety path planning for mobile robot on rough terrain considering instability of attitude maneuver," in *System Integration (SII), 2010 IEEE/SICE International Symposium on*, pp. 55 –60, Dec. 2010.

[6] T. Yoshida, K. Nagatani, E. Koyanagi, Y. Hada, K. Ohno, S. Maeyama, H. Akiyama, K. Yoshida, and S. Tadokoro, "Field experiment on multiple mobile robots conducted in an underground mall," *Field and Service Robotics*, 2009.

[7] S. H. Richard, R. Volpe, P. Backes, J. Balaram, R. Welch, R. Ivlev, G. Tharp, S. Peters, T. Ohm, R. Petras, and S. Laubach, "The rocky 7 rover: A mars sciencecraft prototype," in *Proceedings IEEE International Conference on Robotics and Automation*, pp. 2458–2464, 1997.

[8] K. Nagatani, N. Tokunaga, Y. Okada, and K. Yoshida, "Continuous acquisition of three-dimensional environment information for tracked vehicles on uneven terrain," in *IEEE International Workshop on Safety, Security and Rescue Robotics, 2008. SSRR 2008.*, pp. 25 –30, 2008.

[9] S. Thrun, W. Burgard, and D. Fox, *Probabilistic Robotics (Intelligent Robotics and Autonomous Agents)*. The MIT Press, 2005.